PROMOTING CIRCULAR ECONOMY IN CAST IRON PRODUCTION THROUGH CO-CHARGING OF MILL SCALE–BIOCHAR AGGLOMERATES AND SCRAP IN AN INDUCTION FURNACE

Gianluca Dall'Osto, Davide Mombelli and Carlo Mapelli
Dipartimento di Meccanica, Politecnico di Milano, Via La Masa 1, 20156 Milano, Italy

Carsten Gondorf and Christian Wuppermann
Department for Industrial Furnaces and Heat Engineering, RWTH-Aachen University, Kopernikusstraße 10, 52074 Aachen, Germany

Mahan Firoozbakht and Martin Commer
Foundry Institute, RWTH-Aachen University, Intzestraße 5, 52072 Aachen, Germany

https://doi.org/10.1007/s40962-026-01945-z

Abstract

For ferrous foundries, sustainability is becoming an essential goal to preserve their competitiveness in producing cast iron. Among the possibilities applicable to the iron and steel industry, the charging of alternative iron sources inside the furnaces could represent an effective approach. Following the paradigms of recycling metallurgical residues and the valorization of non-fossil carbon sources, this study examined the use of mill scale–biochar agglomerates as a complementary iron source for producing gray cast iron in induction furnaces. The effect of the agglomerates co-charging (7 wt.% of the total charge) was hence evaluated based on the melt evolution, process yields, and casting product characteristics. The results highlighted the possibility of recovering more than 90 wt.% of the iron contained in the mill scale without affecting the metallic yield (94.6 wt.%) and maintaining the slag production within acceptable levels (2.2 wt.%). Furthermore, the properties of the produced cast iron resulted compliant with those of unalloyed cast iron. Nevertheless, interactions between the agglomerate components and the melt were observed. Compared to the chemical composition of the charged scrap cast iron, the elemental concentrations of carbon, silicon, manganese, and chromium increased in the produced cast iron due to the transfer of these elements from the biochar and mill scale to melt. Similarly, the formation of a diopside-based slag was associated with the introduction of calcium into the melt by biochar. Overall, the results suggested that mill scale, when agglomerated with biochar, can be used as a complementary iron source in the foundry industry.

Received: 15 November 2025 / Accepted: 28 February 2026
Published online: 17 March 2026

Graphical Abstract

Keywords: *carbon composite agglomerates, secondary raw materials, sustainability, cast iron, biochar charging, iron recovery*

Introduction

The development of new sustainable production processes and practices has become an essential issue for most of the hard-to-abate sectors. Among these, the iron and steel industry (ISI) currently accounts for approximately 8% of the global anthropogenic CO_2 emissions.[1] As a consequence, the research efforts have focused primarily on the technological advancements within steelmaking plants and, to a lesser extent, on the mitigation strategies for the foundry industry.[2–4] Nevertheless, foundries represent a key component of the European ISI, producing both ferrous and non-ferrous metal casting that reached 14.5 million tons in 2023, with Germany and Italy together accounting for nearly 70% of this output. Moreover, foundries play an essential role in the energy transition toward renewable energy, as critical components such as gears, shafts, and hubs for wind turbines are manufactured through casting processes.[5] Similar to steelmaking plants, however, foundry processes are characterized by high energy consumption and significant emissions of dust, amines, volatile organic compounds, and CO_2.[6]

When the focus is set on the ferrous metal casting, cupola and induction furnaces are the two main technologies currently in widespread use. According to the 2024 Best Available Techniques (BAT) Reference Document for the Smitheries and Foundries Industry (SF BREF),[7] approximately 50% of iron castings in Western Europe are produced in cupola furnaces. These furnaces use fossil fuels, in the form of foundry coke, to heat the metallic charge (e.g., scrap, pig iron, and alloy materials) up to its melting as well as increase the carbon content of the melt to over 3 wt.% to compensate the charging of excessive amounts of scrap with a low-carbon content (0.1–0.2 wt.%). Consequently, as most of the CO_2 emissions in the smelting process stem from coke utilization, the possibility of reducing the direct greenhouse gas emissions (Scope 1) through the charging and injection of biogenic carbon sources (e.g., raw biomass or biochar) has been argued in recent years.[8,9] Therefore, for a better understanding of substitution rates, the individual emission factors for each fuel are determined based on their carbon content (e.g., from fuel analysis data), and properly managing these carbon sources can drastically decrease the emissions associated with the process, thus favoring its sustainability.[10,11] For example, the industrial scale tests carried out by Echterhof et al.[12] confirmed the possibility of saving up to 10% of the coke charge, albeit at the cost of an increased chamber temperature, a discontinuous injection of biochar

due to its higher reactivity with respect to coke, and the need to use high-quality biochar (volatile matter to fixed carbon ratio of 1:4) to avoid excessive gasification. Furthermore, the results indicated that the introduction of biochar-based agglomerates in cupola furnaces would require an improvement in their mechanical strength to match that of foundry coke. To address this issue, Mousa et al.[13] agglomerated two biochar of increasing quality with coke breeze using several organic binders, additives, and cement. The optimal recipe was found to be a mixture of 62 wt.% biochar, 20 wt.% molasses, 10 wt.% lime and 8 wt.% cement compacted at 160 MPa. Nevertheless, the optimum amount and category (organic vs. inorganic) of binder vary as a function of the compaction method, agglomerate dimensions, and physicochemical properties of the biochar.[14,15]

In contrast, induction furnaces use the circulation of alternating current (AC) in a coil outside the furnace to create a strong magnetic field that inductively heats the metal charge (e.g., scrap metal, pig iron, and in rare cases, sponge iron), eliminating the need for carbon combustion and nearly eliminating most direct emissions (Scope 1).[16] Two specific categories of induction furnaces can be identified: channel induction furnaces and coreless induction furnaces. The former is designed for holding operations, while the latter is designed to achieve short melting times of the metallic charge. To date, coreless induction furnaces are gaining more and more attention as candidates to replace the smaller cupola furnaces in cast iron foundries, hence becoming the future main production technology.[17] Regardless of the induction furnace category, the sustainability of the process is largely dependent on the emissions associated with the production of electricity and is defined as indirect emissions (Scope 2).[5,18–20] These are calculated by multiplying the specific energy consumption of the process by the emission factors corresponding to the electricity mix used.

Concurrently, Abdelshafy et al.[21] evaluated the impact of secondary resources (Scope 3) on the total emissions of the coreless induction process in the German context. In the reference case, consisting of a 1:5 mass ratio of pig iron to waste ductile iron with no steel scrap added, a total of 1031 kg of CO_{2eq} was emitted per ton of liquid cast iron. In contrast, the lowest emissions (837 kg of CO_{2eq} per ton of liquid cast iron) were achieved when the metallic charge consisted solely of steel scrap and waste ductile iron at a mass ratio of 1:2.5, even though a greater amount of carburizing agent was required (0.486 kg versus 10.559 kg). In both cases, Scope 2 emissions remained constant at approximately 500 kg of CO_{2eq} per ton of liquid cast iron. Sappinen et al.[22] expanded the research even further by gathering primary industrial data via questionnaires sent directly to five foundries (two in Finland, one in Germany, one in the Czech Republic, and two in China) with the aim to evaluate the impact of metallic charge sourcing location (e.g., outsourced versus internal return scrap) on the overall emissions. On the one hand, their results confirmed Abdelshafy et al.[21] calculations in the German context. On the other hand, they found that Finnish foundries had the lowest climate impact and Chinese foundries had the highest climate impact, at approximately 750 and 2340 kg of CO_{2eq} per ton of liquid cast iron, respectively. Consequently, they argued that these differences were primarily due to regional variations in the recycling rates of the charging materials as well as the availability and share of renewable and non-renewable energy sources across Northern Europe, Central Europe, and East Asia.

Based on the above considerations and inspired by the positive results obtained by charging self-reducing briquettes in both electric arc furnaces[23–25] and blast furnaces[26] for the iron recovery from oxide-bearing residues, this study provides a first proof-of-concept for the charging feasibility of biogenic carbon composite agglomerates (CCA) inside a coreless induction furnace to produce cast iron. Furthermore, following a waste-to-value philosophy, mill scale was chosen as iron oxide-bearing matrix and agglomerated with biochar. The decision to use mill scale instead of iron ore was supported by its industrial significance. To date, 15–20 kg of mill scale is generated per ton of steel, which is then sold externally at low prices or dumped rather than being valorized as secondary source of strategic elements for the ISI (e.g., Fe, Cr, Mn).[27] On the other hand, using biochar as a reducing agent allows to address the emissions that would be related to the use of a fossil carbon source. Consequently, the focus was set on the metallurgical properties of the produced cast iron, the mineralogy of the slag and its valorization, the amount of

Table 1. Chemical and Mineralogical Composition of Mill Scale

Chemical composition (wavelength-dispersive X-ray fluorescence)									
Element (as oxide)	Al_2O_3	CaO	Cr_2O_3	CuO	Fe_2O_3	MgO	MnO	NiO	SiO_2
wt.%	0.3	0.32	0.45	0.1	96.95	0.07	1.13	0.08	0.6
Mineralogical composition (Rietveld method)									
Mineral phase		Wustite (FeO)			Magnetite (Fe_3O_4)			Hematite (Fe_2O_3)	
wt.%		60			30			10	

Table 2. Proximate Analysis, Ultimate Analysis, and Ash Chemical Composition of Biochar

Parameter/element	Proximate analysis				Ultimate analysis[c]				
	Moisture[a]	Ash[b]	Volatile matter[b]	Fixed carbon[c]	C	H	N	S	O
wt.%	<3	<4	65	35	60	5	1	0.1	35
Element (as oxide)	Ash composition								
	SiO_2	CaO	K_2O	MgO	Na_2O	Others			
wt.%	25	40	20	5	3	7			

a: as received, b: dry basis, c: dry and ash-free basis

iron recovery from mill scale, and the overall effect of the CCA-scrap co-charging practice on the melting process.

Materials and Methods

Biogenic Carbon Composite Agglomerates Materials

The iron oxide-bearing matrix used in this study, mill scale, was collected from an Italian electric arc furnace plant after the rolling processes of steel slabs. Specifically, de-oiling and drying treatments were performed after its collection. Its characterization and reduction feasibility were discussed in a previous work of the author.[14] The chemical composition of the scale was analyzed by means of wavelength-dispersive X-ray fluorescence (Bruker S8 TIGER spectrometer from Bruker AXS GmbH, Karlsruhe, Germany), while the mineralogical composition was determined by Rietveld refinement software (SmartLab Studio II, Rigaku Corporation, Tokyo, Japan). The results are presented in Table 1.

The carbon-bearing matrix, which acted as reducing agent for the mill scale, was a commercial biochar powder of torrefied fresh wood chips (torrefaction temperature 350 °C). In Table 2 are presented the proximate and ultimate analysis results declared by the producer, as well as the ash chemical composition.

The particle size distribution of the mill scale and biochar was investigated by sieve analysis. The results are presented in Table 3. Since the mill scale was almost entirely below 2 mm (96.62 wt.%), no preliminary grinding process was carried out. Similarly, as the biochar was almost entirely below 1 mm (99.01 wt.%), it did not undergo a preliminary grinding process.

Finally, the binder used was a commercial, pre-gelatinized wheat starch designed specifically for technical applications, including the compaction of biogenic and mineral matrices. This was done to minimize the environmental impact of CCAs manufacturing and their subsequent use, thanks to the binder organic nature.[14,15]

Table 3. Particles Size Distribution of Mill Scale and Biochar

Sieve opening (mm)	Passing portion (wt.%)	
	Mill scale	Biochar
> 2	3.38	0.35
2–1	20.48	0.64
1–0.5	25.26	5.36
0.5–0.125	36.74	54.11
< 0.125	14.14	39.54

Design of Biogenic Carbon Composite Agglomerates Recipe and Manufacturing

To ensure the self-reducing ability of the CCA manufactured in this work, the mass of biochar per kg of mill scale was dosed according to the following:

$$\frac{\text{Biochar}(kg)}{\text{Millscale}(kg)} = \frac{Fe_2O_{3\_XRF} \times \sum_i C(i) \times Fe(i)_{RA}}{C_{\text{tot}}} \quad \text{Eqn. 1}$$

where $Fe_2O_{3\_XRF}$ is the amount of iron oxide evaluated through WD-XRF analysis, $Fe(i)_{RA}$ is the amount of iron in the *i-th* oxidative state (II: FeO, III: Fe_2O_3, II+III: Fe_3O_4) evaluated through Rietveld analysis, $C(i)$ is the stoichiometric amount of elemental carbon required for the reduction of iron in the *i-th* oxidative state and C_{tot} the total carbon contained in the biochar evaluated through ultimate analysis. In addition, it should be noted that although the organic carbon contained in the binder can contribute to the reduction process to a lesser extent, this was not considered in the recipe design.

Accordingly, biochar and mill scale (1:3 mass ratio) were inserted in a LM-3e counterflow intensive mixer (Multiserw-Morek, Brzeźnica, Polska). The agitator and mixing drum speeds were set to 2820 and 60 rpm, respectively, to

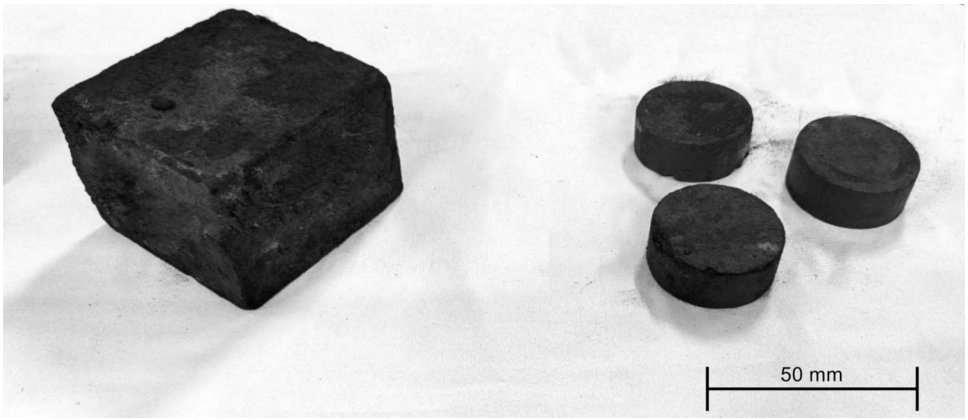

Figure 1. Visual appearance of cured carbon composites agglomerates (either in brick or tablet morphology) made in mill scale and biochar.

Table 4. Biogenic Carbon Composite Agglomerate Composition (wt.%)

Component	Mill scale	Biochar	Binder (gelatinized)
wt.%	67.1	20.6	12.3

crush any clumped particles. After approximately 30 minutes of mixing, the binder was added to match the 7 wt.% of the mixture and the agitator and mixing drum speed decreased to 200 and 4 rpm, respectively. Water required for the initiation of the binder gelatinization was slowly added to the mixture up to reach a relative mass ratio of 1:0.78 respect to the binder. At time intervals of 5 minutes, the material that adhered to the drum was removed using a spatula and reintroduced in the mixture to maximize the homogeneity. The overall process took 60 minutes for the agglomeration of 140 kg of mixture.

The mixture was agglomerated into bricks weighing about 410 g with dimensions of 70×70×30 mm and tablets weighing about 70 g with a diameter of 40 mm and a height of 20 mm (Figure 1) using a Gabbrielli GT2244 hydraulic press (Gabbrielli Technology, Calenzano, Italy) and a Herzog HTP40 semi-automatic pellet press (Herzog Maschinenfabrik, Osnabrück, Germany), respectively.

The compression pressure chosen was 100 MPa with a holding time of 10 s, while a curing process was carried out to allow the expulsion of excess water from the binder. The final composition of CCA after overnight curing at 80 °C in a ventilated oven is shown in Table 4.

Melting Trial Setup and Melting Behavior

To conduct the melting trial, the CCAs in both brick and tablet forms were charged with scrap cast iron in an amount equal to 7 wt.% of the total charge mass. To isolate the effect of CCAs co-charging on the characteristics of the casting products and the overall melting behavior, no additives (e.g., foundry alloys, conditioners, inoculants, and recarburizers) were used. Consequently, the melting trial charge consisted of about 2.3 kg of agglomerates and 30.9 kg of scrap cast iron. The average chemical composition of the latter was evaluated by means of optical emission spectrometry (OES) using an OE750 metals analyzer (Hitachi, Tokyo, Japan). The results are provided in Table 5.

The materials were charged inside a resin-bonded, silicon-carbide crucible (Aug. Gundlach KG, Großalmerode Germany), which was then placed inside a 100-kW coreless induction furnace (Otto Junker, Simmerath, Germany) and operated at its nominal frequency of 900 Hz in air atmosphere. To prevent the agglomerates from floating prematurely due to their lower density compared to molten cast iron, they were placed at the bottom of the crucible (Figure 2).

The melting behavior was visually monitored to determine the time required for the charge to fully melt and to observe any notable phenomena. During the initial stages of heating, the temperature of the solid charge was estimated using an infrared pyrometer. Once the charge melted, the temperature of the bath was measured using thermocouples for temperature measurement of iron and steel melts. After the bath had fully homogenized, the slag was manually skimmed off and collected on a metal platform. Meanwhile, the melt was poured into graphite-coated cast iron molds with external dimensions of 39×15.5×8 cm and internal dimensions of 34.5×10.5×6 cm. Both the slag and the melt samples were cooled down to room temperature in

ambient air and weighed after solidification. Additionally, an OES sample of disk geometry was produced by pouring a small portion of the final melt into a two-piece copper mold. The sample had a diameter of 50 mm and a thickness of 5 mm, and the schematics of the copper mold were similar to those presented in.[28]

Cast iron and Slag Characterization

The produced cast iron was prepared for metallography analysis by traditional grinding, polishing, and etching with 2 wt.% Nital. The microstructure was evaluated by observing the cast iron cross section through a Nikon Eclipse LV150NA optical microscope (Nikon Corporation, Tokyo, Japan) and a Zeiss Sigma 300 field emission gun scanning electron microscope (FEG-SEM) equipped with an Oxford Xmax Ultim 65 energy-dispersive X-ray spectroscopy (EDS) probe (Carl Zeiss AG, Jena, Germany). The average interlamellar spacing of pearlite was evaluated from the post-processing of SEM micrographs in ImageJ software (version 1.53t) according to the methodologies of Vander Voort and Roósz Roósz.[29] Similarly, graphite classification was performed according to the ISO 945-1:2019.[30] The general chemistry was evaluated by OES and performed using a Bruker Q4 Tasman spectrometer (Bruker, Billerica, USA). Finally, the macrohardness of the produced cast iron was evaluated according to ISO 6506-1:2014[31] using an Ernst Twin R/SR durometer (Cisam-Ernst s.r.l., Induno Olona, Italy) equipped with a Brinell indenter.

The collected slag was ground to a particle size of less than 100 μm and its mineralogy investigated by X-ray diffraction (XRD) using a Rigaku SmartLab SE diffractometer (Rigaku Corporation, Tokyo, Japan) with CuKα radiation (λ = 1.54 Å) and a 1D XRF suppression detector (D/Tex 250). The diffraction spectrum was acquired from 10 to 90° 2θ at a scanning rate of 1° min^{-1} with a step size of 0.02° and a rotation speed of 60 rpm to minimize texture effects. Additionally, the elemental distribution within the slag matrix was observed using SEM-EDS maps.

Process Yields

The mass of each element introduced by the charging material at the beginning of the melting trial was estimated by multiplying the mass of the latter by the respective elemental concentration. The elemental distribution (D) was evaluated as follows:

Table 5. Chemical Composition of the Charged Scrap Cast Iron

Element	C	Si	Mn	P	S	Cr	Mo	Mg	Cu	Others[a]	Fe
wt.%	3.510	1.860	0.081	0.025	0.002	0.072	0.007	0.001	0.097	0.011	Balance

a: V, Nb, Al

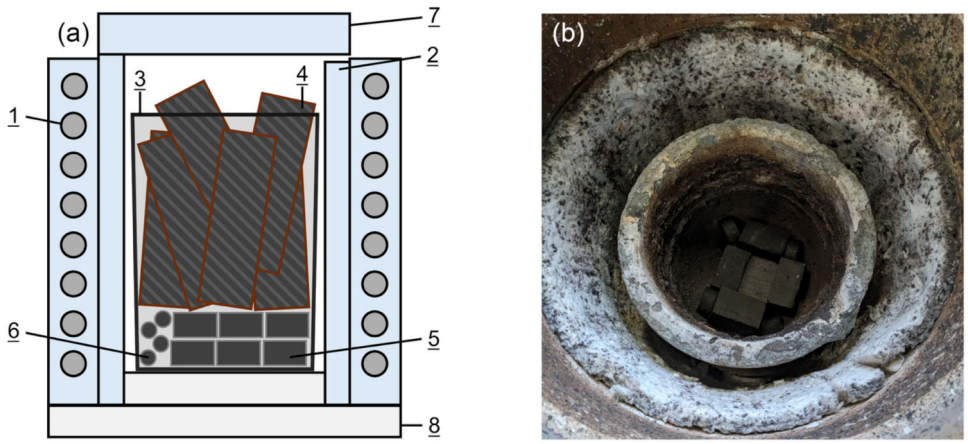

Figure 2. Melting trial setup, (a) overall schematics and (b) photograph of the agglomerates prior to charging the scrap cast iron (1—induction coil, 2—furnace refractory lining, 3—crucible, 4—scrap cast iron, 5—brick agglomerates, 6—tablet agglomerates, 7—induction furnace lid, and 8—refractory basement).

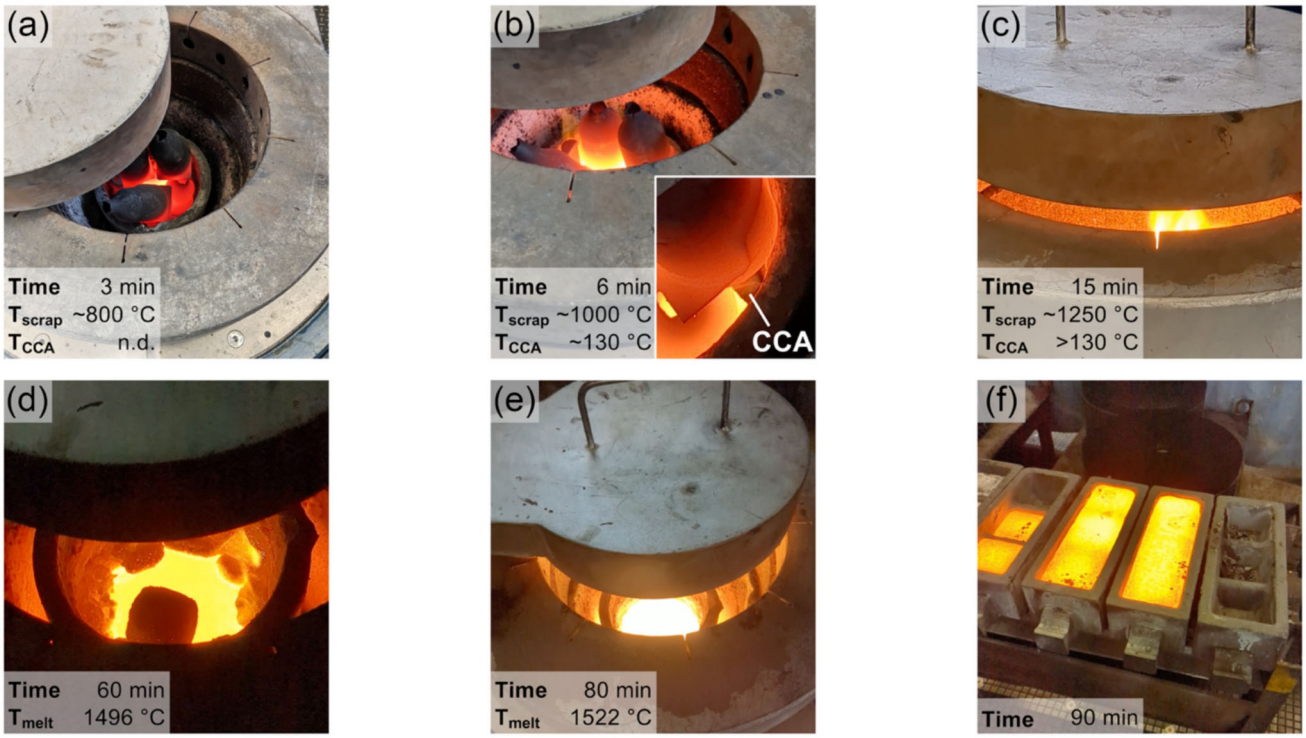

Figure 3. Timestamps of the melting trial (a) start of the melting, (b) start of the carbon composite agglomerates (CCAs) ignition, (c) hot heel generation and combustion of CO released from the iron oxide reduction, (d) floating of the CCAs over the melt, (e) melt homogenization, and (f) melt poured inside the molds. (T_{scrap}: temperature of the scrap cast iron, T_{CCA}: estimated temperature of CCAs, T_{melt}: temperature of the melt).

$$D_{j,i}(wt.\%) = \frac{m_i \cdot w_j}{m_{\text{scrap}} \cdot w_j + m_{\text{MS}} \cdot w_j + m_{\text{BC}} \cdot w_j} \quad \text{Eqn. 2}$$

where m_i is the mass of the *i-th* charging material, m_{scrap} is the mass of charged scrap cast iron, m_{MS} and m_{BC} are the masses of mill scale and biochar contained in the CCA recipe, respectively, and w_j is the *j-th* element concentration. The same methodology was used to evaluate the mass and distribution of each element in the casting products.

The recovery yield of the iron contained in the mill scale was evaluated as follows:

$$\text{Recovery yield}(\%) = \frac{m_{\text{cast}} \cdot w_{\text{Fe}}}{m_{\text{scrap}} \cdot w_{\text{Fe}} + m_{\text{MS}} \cdot \chi_{\text{FeOx}\rightarrow\text{Fe}}} \quad \text{Eqn. 3}$$

where m_{cast} is the experimental mass of the produced cast iron, w_{Fe} is the iron content of produced and charged cast iron evaluated by OES, and $\chi_{FeOx\rightarrow Fe}$ is the conversion factor describing the total amount of recoverable iron from the mill scale used in this work. Finally, the metallic yield of the process was evaluated as the ratio of the cast iron mass to the mass of the charge used for the melting trial.

Results and Discussion

Melting Behavior Observation

Figure 3 shows the most significant timestamps describing the evolution of the melt. Only the scrap cast iron was affected by the electromagnetic field generated by the induction furnace. The temperature reached approximately 800 °C after three minutes and 1000 °C after six minutes. Consistent with the measured temperatures, the surface appeared cherry red and bright yellow, respectively (Figure 3a, b). Conversely, the CCAs maintained their dark color, suggesting low susceptibility to the electromagnetic field and limiting their heating to that transferred from the scrap cast iron. Nevertheless, this heating was sufficient to ignite the biochar powders on the surface, as evidenced by flames arising from the bottom layer of the crucible (Figure 3b). Consequently, in accordance with the producer technical sheet and literature on the self-ignition temperature of torrefied biochar, the estimated temperature reached by the CCA after six minutes was approximately 130 °C.[32] After 15 minutes from the start of the trial, the scrap cast iron reached its melting temperature (approximately 1250 °C) and started to form a hot heel. Concurrently, the flames increased in intensity, suggesting an increase in the temperature of the CCAs as well (Figure 3c). This was likely due to the continued biochar combustion or the post-combustion of the carbon monoxide released by the

reduction of iron oxides contained in the CCAs ($Fe_xO_{y(s)}+C_{(s)}=Fe_xO_{y-1(s)}+CO_{(g)}$, $CO_{(g)}+O_{2(g)}=CO_{2(g)}$).[33,34]

Despite the generation of stirring forces during the subsequent melting of the scrap cast iron (measured temperature: 1496 °C), the buoyant force associated with the lower density of the CCAs compared to the melt (approximately 2.8 vs. 6.69 g cm^{-3}) caused the CCAs to rise and float over the surface (Figure 3d).[35] This phenomenon aligns with Yang et al.[36] experience with agglomerate melting in an electric arc furnace. It represents the main shortcoming that must be addressed before the industrial consolidation of the co-charging practice of CCAs can occur. Since CCAs are intended to be ready-to-use charging materials, the solution must lie in optimizing their properties. For instance, the density of CCAs can be increased through higher compaction forces and improved particle size distribution.[37] However, the intrinsic lower density of the mill scale (5.30 g cm^{-3}) and biochar (0.30 g cm^{-3}) used in this work respect to that of the melt hinders the effectiveness of this method, as it would only delay, and not prevent, the CCAs floating. A more efficient solution would be to add small amounts of metallic swarf or dust into the initial recipe to enhance the CCAs induction susceptibility. This would solve the aforementioned issue of limited CCA heating during the initial melting period. To the authors knowledge, despite this approach has been used successfully to improve the induction self-healing efficiency of oxidic compounds,[38] it has not yet been investigated to enhance the induction melting of CCAs. One final possibility is to use high-reactivity biochar to enhance the reduction kinetics of iron oxides contained in mill scale.[39–41] This would accelerate the recovery and dissolution of iron in the melt, thereby reducing the overall melting time.

Over the following minutes, the CCAs slowly dissolved and the melt was fully homogenized only after 80 minutes from the start of the trial (Figure 3e). The measured temperature was 1522 °C. For reference, the time required by the same experimental setup and melting parameters (e.g., scraps chemistry and amount, furnace power, and frequency) to melt and homogenize a scrap-only charge at 1520 °C is about 45–60 minutes. Therefore, if the properties of the CCAs are not optimized to suppress their floating and their accelerate dissolution, the CCAs co-charging practice will potentially increase the energy demand of the melting process by 1.3–1.7 times compared to a scrap-only melt. Consequently, while this work experimentally investigated the melting behavior of CCAs and their effects on the casting products, the consequences of this practice must also be evaluated through environmental assessments. Despite that this will be the main focus of a dedicated follow-up study, it is already possible to draw some insights based on the literature regarding the use of biochar in electrical steelmaking. For instance, the increase in indirect emission, due to higher energy demand, could be offset by the direct emission savings from using biochar instead of fossil sources as reducing agent in CCAs.[42] As discussed below, since biochar can partially carburize the melt, it can be argued that a lower amount of recarburizers would be needed, thereby mitigating the associated environmental impact and melt costs, as well.[43,44]

Finally, the slag was manually skimmed and left to cool on a metal platform, whereas the molten metal was poured into molds to solidify into ingots (Figure 3f). For completeness, a disk sample was collected for OES analysis by pouring and solidifying part of the final melt into a secondary copper mold.

Products Characterization

Cast iron Characterization

Figure 4 shows the visual appearance of the produced cast iron ingot, the area used for microstructural and macrohardness analysis, and the micrographs taken at increasing magnifications using optical and scanning electron microscopes, respectively. The microstructure is consistent with that of hypereutectoid gray cast iron, which is characterized by thick flakes of primary graphite and thin lamellae of eutectoid graphite (Figure 4c) dispersed in a ferrite and pearlite matrix (Figure 4d). As expected from the higher carbon concentration in these regions, pearlite was observed near the graphite lamellae (Figure 4e). The analysis of the micrographs revealed an average pearlite interlamellar spacing of 300±85 nm, while the graphite was found to be consistent with the characteristics of type I, class A and C gray cast iron as defined in ISO 945-1:2019.[30]

Table 6 shows the chemical composition and Brinell macro-hardness of the cast iron as determined by the previously taken OES sample and the ingot section (Figure 4b), respectively.

To investigate the effect of CCAs co-charging, a comparison was made between scrap and produced cast iron chemical composition. An increment in the carbon and silicon content, from 3.510 to 3.890 wt.% and from 1.860 to 2.089 wt.%, was noted. These increases were related to the dissolution of the biochar particles in the CCAs in the melt, which acted as both a carburizing and an acidic agent. Specifically, the biochar fixed carbon fulfilled the former role, and the silicon in its ash fulfilled the latter role (Table 2). Furthermore, considering the biochar particle size distribution (Table 3) and the overall evolution of the process, it can be assumed that the dissolution occurred in the final stages of melting, which is consistent with the theoretical description of bath recarburization suggested by Umpleby.[45]

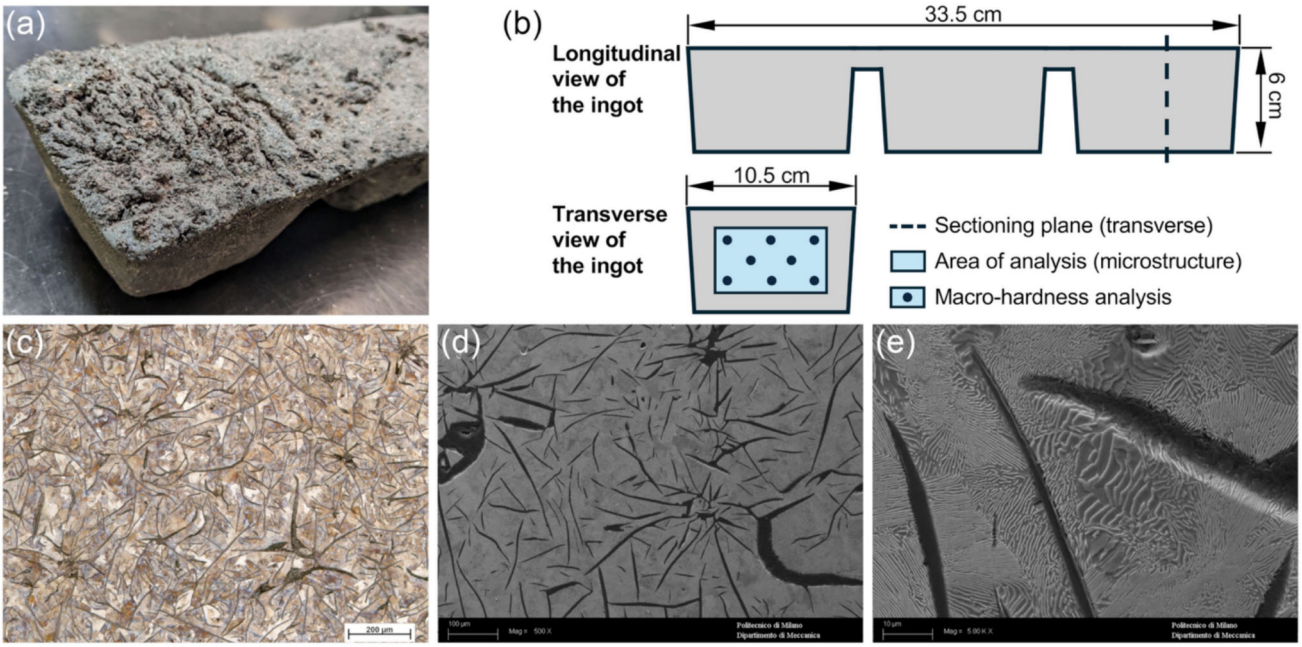

Figure 4. Produced cast iron (a) visual appearance, (b)general ingot dimensions and position of the analysis area, and respective microstructure micrographs taken by (c) optical microscopy (100× magnification), (d) SEM-BSE (500× magnification), and (e) SEM-BSE (5000× magnification) after etching with Nital 2%.

Table 6. Chemical Composition of the Produced Cast Iron and Brinell Macro-Hardness (HB)

Element (wt.%)											HB
C	Si	Mn	P	S	Cr	Mo	Mg	Cu	Others[a]	Fe	
3.890	2.089	0.119	0.026	0.005	0.091	0.007	0.000	0.099	0.009	Balance	157

a: V, Nb, Al

Concurrently, the increase in manganese and chromium content, from 0.081 to 0.119 wt.% and from 0.072 to 0.091 wt.%, was attributed to the transfer of these elements from the mill scale to the melt. Although, a slight increase in sulfur content was observed (0.002 vs. 0.005 wt.%), no significant changes in phosphorus and other main alloying elements were noted. Overall, the chemistry of the produced cast iron was within the expected range for unalloyed cast iron, except for manganese and sulfur, which were below the expected values of 0.2–1.0 wt.% and 0.02–0.25 wt.%, respectively.[46] In this regard, it should be noted that the achieved ratio of manganese to sulfur (Mn:S = 23.8) significantly exceeded the recommended value for preventing iron sulfide precipitation (Mn:S = 1.7).[47] Indeed, the latter is an undesired low melting compound and responsible for hot shortness in gray cast iron. Furthermore, in accordance with the findings of Gundlach,[48] since the product of the total manganese and sulfur content (Mn×S = 0.0006) was below the solubility limit of manganese sulfides in cast irons (Mn×S = 0.3), both elements remained trapped in the ferrite matrix during cooling rather than precipitate as manganese sulfides. This was also confirmed by the absence of such non-metallic inclusion in the microstructure.

Finally, the achieved macro-hardness of 157 HB was consistent with the results reported by El Sawy et al.[49], Vadiraj and Tiwary,[50] Singhal and Saxena,[51] and Du et al.[52] for gray cast irons with similar chemical compositions and microstructures to those in this study. Concurrently, although the achieved value was fully compliant with the depicted macro-hardness value of unalloyed gray cast iron in ISO 185:2020,[53] it fell within the lower range. This behavior was associated with three main factors related to the achieved microstructure and chemistry. First, the significant presence of soft primary graphite (15.423 vol.%) rather than hard carbides.[49,50] Second, the achievement of a coarse pearlite interlamellar spacing of approximately 300 nm. This decreased the respective structural constituent hardness due to the inverse relationship between the hardness and interlamellar spacing of pearlite.[52,54] Third, the low amount of manganese and sulfur. Indeed, when present in higher amounts than those achieved in this study and carefully dosed to avoid negative

sulfur-related effects, these elements improve the mechanical properties of cast iron.[48,49] Therefore, based on the above discussion of the effects of CCAs co-charging on the achieved chemistry and cast iron microstructure, it can be concluded that this practice can indirectly affect the mechanical properties of the produced cast iron.

Slag Characterization and Following Valorization

Figure 5 shows the visual appearance, diffraction pattern and SEM-EDS maps of the slag. As expected for a foundry ferrous slag sample achieved by an induction furnace,[55] the cooled slag surface color ranged from dark green to black, with a vitreous and dull luster (Figure 5a). Additionally, small metal droplets were observed along the surface and within the slag matrix. Their amount was determined by crushing and mechanically separating the metallic and non-metallic phases of some of the collected slag samples. According to Hartung et al.[56], the achieved result of 3.28 wt.% falls within the acceptable range of metallic phases contained in foundry slag. This also indicates that the manual skimming process was performed correctly, avoiding the introduction of major bias into the mineralogical and chemical characterization of the slag due to the presence of metallic phases. According to the diffraction pattern (Figure 5b), the slag mineralogy consisted primarily of silicon compounds, specifically diopside ($Al_{0.6}CaMg_{0.7}Si_{1.7}O_6$), quartz ($SiO_2$), and cristobalite ($SiO_2$). This composition is consistent with that observed in slag produced during iron reduction in the presence of high silicon-bearing materials, as in this work.[57] Specifically, each of the charge materials contained significant amounts of silicon, which may have been partially oxidized during melting tests. Meanwhile, calcium and magnesium were primarily present in mill scale and biochar. The presence of both metallic iron (Fe) and magnesiowuestite ($Fe_{0.4}Mg_{0.6}O$) was observed as well. The mineralogical observations were confirmed by the SEM-EDS analysis (Figure 5c). The slag matrix consisted of diopside, with islands of silicon oxides and iron compounds distributed throughout. The chemical composition of the slag was also consistent with that expected from a ferrous foundry slag.[55] In descending order of major constituents: SiO_2 (61.05 wt.%), CaO (13.92 wt.%), MgO (9.85 wt.%), Al_2O_3 (8.86 wt.%), Fe_2O_3 (3.39 wt.%), K_2O 2.19 (wt.%), MnO (0.67 wt.%), and MgO (0.06 wt.%), respectively. It should be noted that the higher amount of potassium in the produced slag compared to traditional ferrous foundry slag can be attributed to the significant presence of such element in the biochar ash.[58]

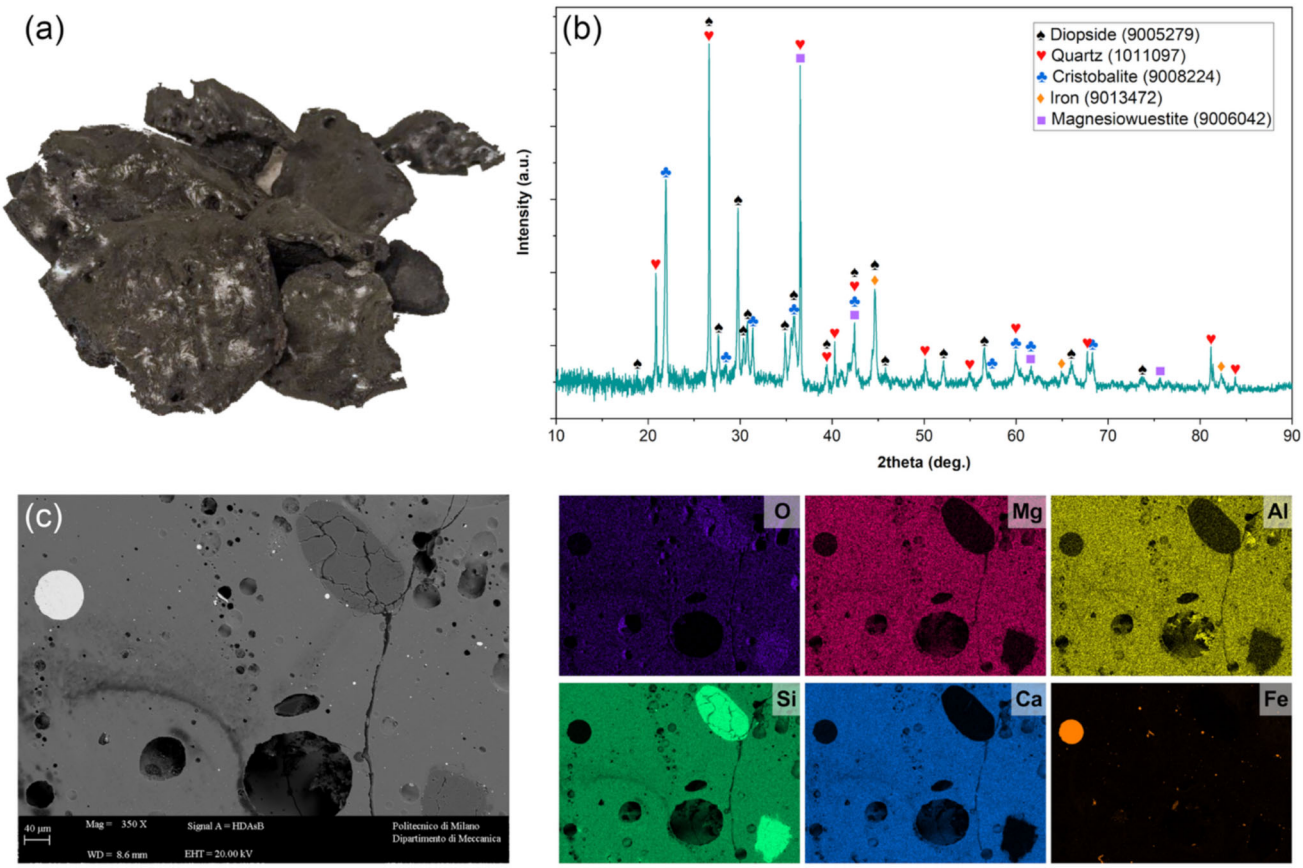

Figure 5. Slag characterization: (a) visual appearance, (b) diffraction pattern (DB card number in parenthesis), (c) SEM-BSE micrograph of the cross section and related SEM-EDS maps.

Consequently, given the inverse relationship between slag basicity ($BI_3 = (CaO + MgO)/SiO_2$) and viscosity, it can be concluded that the primary cause of metallic iron losses in this study was the acidic nature (BI_3 = 0.39) of the slag itself, or, in other words, its high viscosity.[59] This is a well-known problem that affects most metallurgical processes involving skimming and is commonly referred to as colloid losses.[60] Specifically, as proposed by Yang et al.[61] , during melting, the passage of gas bubbles from the melt to the slag is accompanied by the parallel transfer of small, round metal droplets. Consequently, if the slag viscosity is too high and it is not properly lowered before skimming (e.g., by adding slag modifiers or lime), these metal droplets can remain entrapped in the slag itself. In this work, the carbon monoxide, released by the reduction of iron oxides contained in the CCAs, was responsible for the generation of a gaseous phase, whereas the morphology of the iron particles observed in Figure 5c confirmed the mechanism proposed. On the other hand, the presence of magnesiowuestite was likely due to the incomplete reduction of the iron oxides contained in the CCAs and their reaction with magnesium-bearing phases.[14,62]

As detailed in two recently published reviews by Aguiar et al.[63] and Khanom et al.[64], induction furnace slag is primarily valued in the cement sector and as coarse aggregates in the construction industry, where some specific applications, such as in clay brick production[65] and as an antimicrobial agent in building materials,[66] have also been investigated. Nevertheless, as Pribulová[67] has emphasized, the practical utilization of ferrous foundry slag in Europe remains limited due to the small quantity produced per melt, especially if compared to blast and electric arc furnace slag (e.g., up to tens vs. hundreds of kg per ton of charge), as well as its chemical and mineralogical composition. Indeed, the European Standard EN 197-1:2011[68] states that the slag basicity must be greater than one for it to be considered eligible as raw material in cement production. Consequently, the acidic nature of the slag produced negates the above valorization possibility since the formation of calcium and aluminum silicates, which are essential for achieving the desired hydraulic, binding, and mechanical properties of cement would be inhibited.[69] To address this issue and in accordance with the principles of the circular economy, Eckert et al.[70] proposed using lime sludge, a by-product of cellulose production, as a potential basicity corrector in the development of an eco-cementitious material. They found that a 20 wt.% substitution of clinker could be achieved by correcting the slag basicity up to a value of 1.2 without affecting the cement mechanical properties. Conversely, foundry ferrous slag can more easily be used as a sand replacement or aggregate in concrete products. For instance, Devi et al.[71] observed an increase in compressive, split tensile, and flexural strength with a 30 wt.% substitution of sand. Similar results were achieved by Sharma et al.[72] and Cardoso et al.[55], who also observed a decrease in water demand to maintain workability of the concrete. However, they also noted large quantities of gel phases produced by the alkali-silica reaction due to the reactive nature of the aggregates, which in turn is related to the chemistry of the foundry slag itself. Therefore, given the high levels of potassium and silicon in the slag produced in this study, its use as an aggregate in concrete may be limited to low substitution rates.

Elemental Distribution Assessment, Metallic Yield, and Recovery Yield

Figure 6 shows the distribution and mass of the elements introduced by the charging material, as well as the corresponding values observed in the casting products.

The mass balance revealed consistency in the input and output elemental masses, with occasional discrepancies within a 5% margin of error. These discrepancies were considered acceptable from an experimental perspective, confirming the absence of bias in characterizing the casting products and related discussions. The only exception was carbon, whose mass in the solid output was 20% lower than the mass present in the input. This was expected, given the conversion of carbon into gaseous phases during the reduction of iron oxides ($Fe_xO_{y(s)}+C_{(s)}=Fe_xO_{y-1(s)}+CO_{(g)}$, $CO_{(g)}+O_{2(g)}=CO_{2(g)}$).[33,34] Therefore, considering the amount of cast iron produced (31.4 kg), it is possible to estimate that the melting trial emitted approximately 31 g of CO_2 per kg of cast iron. However, it is not possible to determine whether this CO_2 value should be considered fully or partly biogenic due to the concurrent presence of fossil carbon within the scrap cast iron.

Table 7 provides a summary of the charge composition, the mass of cast iron and slag produced, the recovery yield of iron contained in the CCAs and the overall metallic yield of the melting trial.

In accordance with the study of Fedorko et al.[73], which examined the use of foundry dust as a complementary iron source in an induction furnace charge, the CCAs charging lead to a greater amount of slag (0.7 kg) than that expected from the solely contribution of biochar ash and binder (0.35 kg). Specifically, the relative amount of slag was three times higher than that typically observed during melting trials with the same setup as this study for gray cast iron production (2.2 vs. 0.7 wt.%) and only slightly exceeding the benchmark range (1–2 wt.%) indicated in the 2024 BAT SF BREF document.[7] This increase was related to three contributions: (i) the transfer of oxide compounds (e.g., SiO_2, CaO, Al_2O_3, etc.) from the scrap cast iron, biochar ash, or binder into the slag phase rather than their dissolution into the melt as alloying elements, (ii) incomplete reduction of the iron oxides in the mill scale, and (iii) trapping of metallic iron particles in the melt. Nevertheless, it can be also argued that choosing to use an

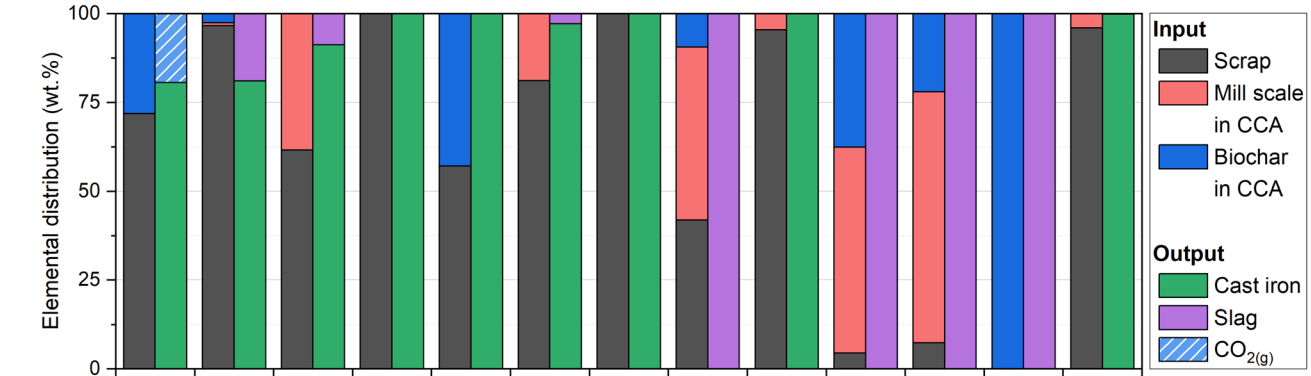

	C	Si	Mn	P	S	Cr	Mo	Mg	Cu	Ca	Al	K	Fe
Input (kg)	1.514	0.674	0.040	0.008	0.002	0.029	0.002	0.001	0.032	0.037	0.013	0.001	30.394
Output (kg)	1.221*	0.704	0.039	0.008	0.002	0.029	0.002	0.001	0.031	0.042	0.012	0.001	29.482

*The value refers solely to the C contained in the solid output, the remaining was removed as gaseous output

Figure 6. Mass balance and distribution of the elements within charging materials (input) and casting products (output).

Table 7. Summary of Charge and Casting Products Masses/Relative Amounts and Process Yields (CCA: Carbon Composite Agglomerates)

Charge composition (kg / wt.%)		Casting products (kg / wt.%)		Yield (%)	
Scrap	CCA	Cast iron	Slag	Recovery	Metallic
30.9/93.1	2.3/6.9	31.4/97.8	0.7/2.2	91.5	94.6

organic binder for the CCAs positively impacted the first contribution by avoiding the introduction of silica, which is typically present in significant amounts in inorganic binders such as bentonite.[74]

The recovery yield of the iron oxide in the mill scale was sufficient (91.5%) to confirm the feasibility of using CCAs as a complementary iron source in an induction furnace, with no effect on the process metallic yield (94%). This is likely due to the decrease of iron oxides activity in the slag, which occurs when biochar carbon dissolves in the melt during the final stages of melting, and hence the parallel protection from bath oxidation.[75] A comparable behavior was also observed by Paknahada et al.[76] during the charging and melting of cold-briquetted iron and carbon (CBIC) in an electric furnace respect to either cold direct reduced iron (CDRI) or hot briquetted iron (HBI).

Conclusion

In the quest for a more sustainable cast iron production and steel residue valorization, this work investigated the feasibility of using carbon composite agglomerates made from mill scale and biochar as a complementary iron source for traditional scrap cast iron in a coreless induction furnace. On the one hand, the melting trial was continuously monitored to evaluate melt behavior under the conditions of simultaneous agglomerates and scrap cast iron ingots charging. On the other, the casting products (cast iron and slag) were characterized metallurgically, chemically, and mineralogically to investigate the effect of agglomerate charging. Finally, the recovery yield of iron in the mill scale was assessed using mass and chemical balances.

The following conclusions were drawn from the achieved results:

- The total time required to heat and melt 30.9 kg of cast iron scrap and 2.3 kg of CCAs was approximately 80 minutes. During the test, the CCAs were unresponsive to the electromagnetic field, limiting their heating to that transferred first by the scrap cast iron and then by the melt itself. Furthermore, the agglomerates lower density compared to the molten material caused them to rise and float three-quarters of the way through the melting process. This prolonged the time required for the molten material to homogenize.
- The addition of CCAs to the charge altered the chemistry of the metallic charge. Specifically, the fixed carbon and silica compounds present in the biochar increased the produced cast iron carbon and silicon content, respectively. Similarly, the manganese and chromium in the mill scale increased the respective values of the cast iron, albeit by a smaller amount.
- Using CCAs in an amount equal to 7 wt.% of the charge mass resulted in an ingot with a microstructure, chemical composition, and macro-hardness compliant with that of unalloyed lamellar gray cast iron. The only exceptions were the final amounts of manganese and sulfur, which were below the typical compositional ranges. However, these values were already below the thresholds in the initial charge.

- The high concentration of calcium compounds in the biochar ash and the significant silicon content of the melt resulted in the formation of a diopside-matrix slag. This matrix contained dispersed islands of unreduced iron (magnesiowuestite), metallic iron, and silicon compounds (either quartz or cristobalite). Still, the amount of slag produced was relatively low and equal to 2.2 wt.% of the total mass of casting products.
- The recovery yield of iron from the mill scale contained in the CCAs was 91.5%, suggesting the possibility of valorizing such residue in the foundry industry as a complementary iron source for the scrap cast iron once it is agglomerated with biochar.

The outcomes of this investigation highlight the potential of carbon composite agglomerates produced from mill scale and biochar as a viable complementary iron source in cast iron melting. Nevertheless, further research is needed to deepen the understanding of the metallurgical phenomena involved and to enhance process robustness. Future studies should particularly address the possibility of further modifying the microstructure of the resulting cast iron, especially the graphite morphology, through optimization of the CCA formulation and melting parameters. Moreover, attention should be devoted to evaluating the repeatability of the melting trials, considering the inherent heterogeneity of the biochar, mill scale, and scrap cast iron employed as charge materials. Finally, a comprehensive assessment of the environmental and economic implications, including potential emission reductions and cost savings associated with this approach, will be essential to substantiate its industrial applicability and its contribution toward a more sustainable foundry practice.

Author contributions Conceptualization was performed by Gianluca Dall'Osto, Carsten Gondorf; methodology by Gianluca Dall'Osto, Carsten Gondorf, Mahan Firoozbakht; formal analysis and investigation by Gianluca Dall'Osto, Carsten Gondorf, Mahan Firoozbakht, Martin Commer; writing—original draft preparation—by Gianluca Dall'Osto, Carsten Gondorf; writing—review and editing—by Gianluca Dall'Osto, Carsten Gondorf, Mahan Firoozbakht, Davide Mombelli, Christian Wuppermann; resources by Carsten Gondorf, Mahan Firoozbakht, Martin Commer; supervision by Mahan Firoozbakht, Davide Mombelli, Carlo Mapelli, Christian Wuppermann.

Funding

Open access funding provided by Politecnico di Milano within the CRUI-CARE Agreement. The author did not receive support from any funding agency in the public, commercial, or not for profit sectors.

Data availability

All the data required are available within the manuscript.

Conflict of interest All authors certify that they have no affiliations with or involvement in any organization or entity with any financial interest or non-financial interest in the subject matter or materials discussed in this manuscript.

REFERENCES

1. V. Shatokha, Injection of hydrogenous gases into the blast furnace tuyeres for reducing CO2 emissions: a review. ISIJ Int. **64**, 1945–1955 (2024). https://doi.org/10.2355/isijinternational.ISIJINT-2024-145
2. T. Ariyama, M. Sato, Optimization of ironmaking process for reducing CO2 emissions in the integrated steel works. ISIJ Int. **46**, 1736–1744 (2006). https://doi.org/10.2355/isijinternational.46.1736
3. R. Higashi, D. Maruoka, Y. Iwami et al., Recycling process for net-zero CO2 emissions in steel production. ISIJ Int. **64**, 1486–1492 (2024). https://doi.org/10.2355/isijinternational.ISIJINT-2024-073
4. T. Ariyama, Perspectives on the promising pathways to zero carbon emissions in the steel industry toward 2050. ISIJ Int. **65**, 165–184 (2024). https://doi.org/10.2355/isijinternational.ISIJINT-2024-320
5. B. Monteleone, E. Baldereschi, N. Fabbri et al., A sustainability assessment of the foundry production process in Italy. Sustain. Prod. Consum. **46**, 491–501 (2024). https://doi.org/10.1016/j.spc.2024.03.005
6. E. Stefana, P. Cocca, F. Marciano et al., A review of energy and environmental management practices in cast iron foundries to increase sustainability. Sustainability **11**, 7245 (2019). https://doi.org/10.3390/su11247245
7. Aries, E., Chronopoulos, G., Schorcht, F., et al. (2024) Best Available Techniques (BAT) Reference Document for the Smitheries and Foundries Industry (SF BREF). Publications Office of the European Union
8. R.M. Torielli, F.S. Cannon, R.C. Voigt et al., The environmental performance and cost of innovative technologies for ductile iron foundry production. Int.

J. Met. **8**, 37–48 (2014). https://doi.org/10.1007/BF03355570
9. M.H. Gabra, R.K. Jain, A. Tiwari, Energy efficient cupola furnace via hybridization with a biomass gasifier. Int. J. Emerg. Technol. Eng. Res. **5**, 54–62 (2017)
10. M. Hammerschmid, S. Müller, J. Fuchs et al., Evaluation of biomass-based production of below zero emission reducing gas for the iron and steel industry. Biomass Convers. Biorefinery **11**, 169–187 (2021). https://doi.org/10.1007/s13399-020-00939-z
11. F. Meng, G. Rong, R. Zhao et al., Incorporating biochar into fuels system of iron and steel industry: carbon emission reduction potential and economic analysis. Appl. Energy **356**, 122377 (2024). https://doi.org/10.1016/j.apenergy.2023.122377
12. T. Echterhof, T. Demus, M. Schulten et al., *Substituting fossil carbon sources in the electric arc and cupola furnace with biochar* (European Steel Environment & Energy Congress Teesside University, UK, 2014)
13. E. Mousa, M. Kazemi, M. Larsson et al., Potential for developing biocarbon briquettes for foundry industry. App. Sci. **9**, 5288 (2019). https://doi.org/10.3390/app9245288
14. G. Dall'Osto, D. Mombelli, S. Scolari et al., Role of the biogenic carbon physicochemical properties in the manufacturing and industrial transferability of mill scale-based self-reducing briquettes. Metals **14**, 882 (2024). https://doi.org/10.3390/met14080882
15. H. Suopajärvi, K. Umeki, E. Mousa et al., Use of biomass in integrated steelmaking – status quo, future needs and comparison to other low-CO2 steel production technologies. Appl. Energy **213**, 384–407 (2018). https://doi.org/10.1016/j.apenergy.2018.01.060
16. G.V.R. Gandhewar, S.V. Bansod, A.B. Borade, Induction furnace–a review. Int. J. Eng. Technol. **3**, 277–284 (2011)
17. I. Riposan, M. Chisamera, S. Stan, Enhanced quality in electric melt grey cast irons. ISIJ Int. **53**, 1683–1695 (2013). https://doi.org/10.2355/isijinternational.53.1683
18. O. Yilmaz, A. Anctil, T. Karanfil, LCA as a decision support tool for evaluation of best available techniques (BATs) for cleaner production of iron casting. J. Clean. Prod. **105**, 337–347 (2015). https://doi.org/10.1016/j.jclepro.2014.02.022
19. J. Mitterpach, E. Hroncová, J. Ladomerský et al., Environmental analysis of waste foundry sand via life cycle assessment. Environ. Sci. Pollut. Res. Int. **24**, 3153–3162 (2017). https://doi.org/10.1007/s11356-016-8085-z
20. J. Mitterpach, E. Hroncová, J. Ladomerský et al., Environmental evaluation of grey cast iron via life cycle assessment. J. Clean. Prod. **148**, 324–335 (2017). https://doi.org/10.1016/j.jclepro.2017.02.023
21. A. Abdelshafy, D. Franzen, A. Mohaupt et al., A feasibility study to minimize the carbon footprint of cast iron production while maintaining the technical requirements. J. Sustain. Metall. **9**, 249–265 (2023). https://doi.org/10.1007/s40831-022-00642-5
22. T. Sappinen, J. Peltokorpi, E. Alieva et al., Comparison of carbon footprints in sourcing of cast components. Inter. Metalcast. **20**, 428–439 (2026). https://doi.org/10.1007/s40962-025-01608-5
23. A. Davydenko, A. Karasev, B. Glaser et al., Direct reduction of Fe, Ni and Cr from oxides of waste products used in briquettes for slag foaming in EAF. Materials **12**, 3434 (2019). https://doi.org/10.3390/ma12203434
24. T. Willms, T. Echterhof, S. Steinlechner et al., Investigation on the chemical and thermal behavior of recycling agglomerates from EAF by-products. Appl. Sci. **10**, 8309 (2020). https://doi.org/10.3390/app10228309
25. M.C. Bagatini, V. Zymla, E. Osório et al., Scale recycling through self-reducing briquettes to use in EAF. ISIJ Int. **57**, 2081–2090 (2017). https://doi.org/10.2355/isijinternational.ISIJINT-2017-242
26. C. Takano, R.C. Nascimento, G.F.BLe. Silva et al., Recycling of solid wastes from integrated steelmaking plant: a sustainable alternative. Mater. Trans. **42**, 2506–2510 (2001). https://doi.org/10.2320/matertrans.42.2506
27. I. Matino, V. Colla, T.A. Branca et al., Optimization of by-products reuse in the steel industry: Valorization of secondary resources with a particular attention on their pelletization. Waste Biomass Valoriz. **8**, 2569–2581 (2017). https://doi.org/10.1007/s12649-016-9768-x
28. M. Laubertova, S. Ruzickova, J. Trpcevska et al., Experimental study of a representative sample to determine the chemical composition of cast iron. Materials **17**, 1255 (2024). https://doi.org/10.3390/ma17061255
29. G.F. Vander Voort, A. Roósz, Measurement of the interlamellar spacing of pearlite. Metallography **17**, 1–17 (1984). https://doi.org/10.1016/0026-0800(84)90002-8
30. ISO 945-1:2019 Microstructure of cast irons. Part 1: Graphite classification by visual analysis. International Standard Organization (ISO), Geneva, Switzerland, 2019. Accessed on 10 February 2026. https://www.iso.org/standard/77568.html
31. ISO 6506-1:2014 Metallic materials – Brinell hardness test. Part 1: Test method. International Standard Organization (ISO), Geneva, Switzerland, 2019. Accessed on 02 October 2025 https://www.iso.org/standard/59671.html
32. F. Restuccia, O. Mašek, R.M. Hadden et al., Quantifying self-heating ignition of biochar as a function of feedstock and the pyrolysis reactor temperature. Fuel

236, 201–213 (2019). https://doi.org/10.1016/j.fuel.2018.08.141
33. O.I. Nokhrina, I.D. Rozhikhina, I.E. Khodosov, Manufacturing and application of metalized ore-coal pellets in synthetic pig iron smelting. IOP Conf. Ser.: Mater. Sci. Eng. **142**, 012068 (2016). https://doi.org/10.1088/1757-899X/142/1/012068
34. H.-H. Chang, I.-G. Chen, K.-M. Lu et al., Effect of heating rate on carbothermic reduction and melting behavior of iron ore-coal composite pellets. ISIJ Int. **61**, 2715–2723 (2021). https://doi.org/10.2355/isijinternational.ISIJINT-2021-175
35. P. Fima, N. Sobczak, Density and surface tension of molten cast irons. J. Min. Metall. B: Metall. **57**, 439–447 (2021). https://doi.org/10.2298/JMMB210413040F
36. Q. Yang, A. Xu, P. Xue et al., Briquette smelting in electric arc furnace to recycle wastes from stainless steel production. J. Iron. Steel Res. Int. **22**, 10–16 (2015). https://doi.org/10.1016/S1006-706X(15)30131-X
37. A.D. Seboka, J. Morken, M.S. Adaramola et al., Optimization of briquetting parameters and their effects on thermochemical fuel properties of biowaste briquettes. Bioresour. Technol. **439**, 133277 (2026). https://doi.org/10.1016/j.biortech.2025.133277
38. C. Yang, S. Wu, J. Xie et al., Enhanced induction heating and self-healing performance of recycled asphalt mixtures by incorporating steel slag. J. Clean. Prod. **366**, 132999 (2022). https://doi.org/10.1016/j.jclepro.2022.132999
39. H. Ahmed, M. Elsadek, M. Lundgren et al., Reduction behavior of biochar-in-plant fines briquettes for CO2-reduced ironmaking. Metals **15**, 973 (2025). https://doi.org/10.3390/met15090973
40. S. Ueda, K. Watanabe, K. Yanagiya et al., Improvement of reactivity of carbon iron ore composite with biomass char for blast furnace. ISIJ Int. **49**, 1505–1512 (2009). https://doi.org/10.2355/isijinternational.49.1505
41. K. Watanabe, S. Ueda, R. Inoue et al., Enhancement of reactivity of carbon iron ore composite using redox reaction of iron oxide powder. ISIJ Int. **50**, 524–530 (2010). https://doi.org/10.2355/isijinternational.50.524
42. Demus, T., Reichel, T., Echterhof, T., et al. Biochar usage in EAF-steelmaking potential and feasibility. 1st European Steel Technology & Application Days (ESTAD) & 31st Journées Sidérurgiques Internationales (JSI), Paris, France (2014)
43. R. Robinson, L. Brabie, M. Pettersson et al., An empirical comparative study of renewable biochar and fossil carbon as carburizer in steelmaking. ISIJ Int. **62**, 2522–2528 (2022). https://doi.org/10.2355/isijinternational.ISIJINT-2020-135
44. L. Testini, A. Misul, V. Morreale et al., Corporate carbon footprint and Scope 3 emissions in stainless steel electric arc furnace steelmaking: a step to tackle climate change. ACS Sustain. Resour. Manag. (2026). https://doi.org/10.1021/acssusresmgt.5c00588
45. R.J. Umpleby, Toward a more complete quantitative model of recarburizer dissolution in liquid iron. Inter. Metalcast. (2025). https://doi.org/10.1007/s40962-025-01744-y
46. J.R. Davis, *ASM Specialty Handbook: Cast Irons*, 1st edn. (ASM International, Materials Park, 1996), pp.32–54
47. R. Srivastava, B. Singh, K.K. Saxena, Influence of S and Mn on mechanical properties and microstructure of grey cast iron: an overview. Mater. Today Proc. **26**, 2770–2775 (2020). https://doi.org/10.1016/j.matpr.2020.02.577
48. R. Gundlach, M. Meyer, L. Winardi, Influence of Mn and S on the properties of cast iron Part III—testing and analysis. Int. Metalcast. **9**, 69–82 (2015). https://doi.org/10.1007/BF03355617
49. E.E.T. El Sawy, M.R. El -Hebeary, I.S.E. El Mahallawi, Effect of manganese, silicon and chromium additions on microstructure and wear characteristics of grey cast iron for sugar industries applications. Wear **390–391**, 113–124 (2017). https://doi.org/10.1016/j.wear.2017.07.007
50. A. Vadiraj, S. Tiwari, Effect of silicon on mechanical and wear properties of aluminium-alloyed gray cast iron. J. Mater. Eng. Perform. **23**, 3001–3006 (2014). https://doi.org/10.1007/s11665-014-1040-6
51. P. Singhal, K.K. Saxena, Effect of silicon addition on microstructure and mechanical properties of grey cast iron: an overview. Mater. Today Proc. **26**, 1393–1401 (2020). https://doi.org/10.1016/j.matpr.2020.02.281
52. S. Du, C. Chen, R. Chen et al., Influence of casting materials on the microstructure and mechanical properties of gray cast iron for cylinder liners. Inter. Metalcast. **19**, 1650–1662 (2025). https://doi.org/10.1007/s40962-024-01413-6
53. ISO 185:2020 Grey cast irons – Classification. International Standard Organization (ISO), Geneva, Switzerland, 2019. Accessed on 04 February 2025 https://www.iso.org/standard/80283.html
54. S.S. Sahay, G. Mohapatra, G.E. Totten, Overview of pearlitic rail steel: accelerated cooling, quenching, microstructure, and mechanical properties. J. ASTM Int. **6**, 1–26 (2009). https://doi.org/10.1520/JAI102021
55. C. Cardoso, A. Camões, R. Eires et al., Using foundry slag of ferrous metals as fine aggregate for concrete. Resour. Conserv. Recycl. **138**, 130–141 (2018). https://doi.org/10.1016/j.resconrec.2018.05.020
56. C. Hartung, M. Liptak, R. Logan et al., Thermochemical evaluation of cast iron slags generated from a holding furnace. Inter. Metalcast. **17**, 2754–2761 (2023). https://doi.org/10.1007/s40962-022-00947-x
57. Z. Tong, J. Sun, J. Wang et al., Iron reduction and diopside-based glass ceramic preparation based on mineral carbonation of steel slag. Environ. Sci. Pollut.

Res. Int. **28**, 796–804 (2021). https://doi.org/10.1007/s11356-020-10358-2
58. C. DiGiovanni, T. Echterhof, Progress toward biocarbon utilization in electric arc furnace steelmaking: current status and future prospects. J. Sustain. Metall. **10**, 2047–2067 (2024). https://doi.org/10.1007/s40831-024-00940-0
59. R. Jia, L. Deng, F. Yun et al., Effects of SiO2/CaO ratio on viscosity, structure, and mechanical properties of blast furnace slag glass ceramics. Mater. Chem. Phys. **233**, 155–162 (2019). https://doi.org/10.1016/j.matchemphys.2019.05.065
60. F.N.H. Schrama, F. Ji, A. Hunt et al., Lowering iron losses during slag removal in hot metal desulphurisation without using fluoride. Ironmaking Steelmaking **47**, 464–472 (2020). https://doi.org/10.1080/03019233.2020.1747778
61. A.F. Yang, A. Karasev, P.G. Jönsson, Characterization of metal droplets in slag after desulfurization of hot metal. ISIJ Int. **55**, 570–577 (2015). https://doi.org/10.2355/isijinternational.55.570
62. A. Vickerfält, J. Martinsson, D. Sichen, Effect of reduction degree on characteristics of slag formed by melting hydrogen-reduced DRI and partitions of P and V between slag and metal. Steel Res. Int. (2021). https://doi.org/10.1002/srin.202000432
63. I. Aguiar, S. Cunha, J. Aguiar, Application of foundry wastes in eco-efficient construction materials: a review. Appl. Sci. **15**, 10 (2024). https://doi.org/10.3390/app15010010
64. R. Khanom, M. Hasanuzzaman, M. Hasanuzzaman et al., Assessment and recycling options of induction furnace steel slag: a review. Environ. Technol. Rev. **15**, 29–39 (2026). https://doi.org/10.1080/21622515.2025.2605448
65. M.J. Miah, M.K. Ali, Y. Li et al., Impact of induction furnace steel slag as replacement for fired clay brick aggregate on flexural and durability performances of RC beams. Materials **14**, 6268 (2021). https://doi.org/10.3390/ma14216268
66. J. Baalamurugan, V. Ganesh Kumar, T. Stalin Dhas et al., Utilization of induction furnace steel slag based iron oxide nanocomposites for antibacterial studies. SN Appl. Sci. **3**, 295 (2021). https://doi.org/10.1007/s42452-021-04299-9
67. A. Pribulová, P. Futáš, M. Bartošová et al., Utilization of slags from foundry process. J. Cast. Mater. Eng. **1**, 103 (2017). https://doi.org/10.7494/jcme.2017.1.4.103
68. BS EN 197-1:2011 Cement. Composition, specifications and conformity criteria for common cements. British Standards Institution (BSI), London, UK, 2011. Accessed on 17 October 2025 https://bsol.bsigroup.com/Bibliographic/BibliographicInfoData/000000000030391002
69. E. L'Hôpital, B. Lothenbach, D.A. Kulik et al., Influence of calcium to silica ratio on aluminium uptake in calcium silicate hydrate. Cem. Concr. Res. **85**, 111–121 (2016). https://doi.org/10.1016/j.cemconres.2016.01.014
70. C.L. Eckert, L. Rosso Neto, C.H. Borgert et al., Design of new eco-cementitious material based on foundry slag and lime sludge. Minerals **15**, 1059 (2025). https://doi.org/10.3390/min15101059
71. S. Devi, S.M. Shahrukh, S. Joshi et al., Utilization of foundry slag as a partial replacement of cement and sand. SSRG Int. J. Civ. Eng. **3**, 80–85 (2016)
72. D. Sharma, S. Sharma, A. Goyal, Utilization of waste foundry slag and Alccofine for developing high strength concrete. Int. J. Electrochem. Sci. **11**, 3190–3205 (2016). https://doi.org/10.1016/S1452-3981(23)16174-8
73. P. Fedorko, A. Pribulova, P. Futas et al., The treatment of iron-containing foundry dusts with the aim of their recycling and their effect on the properties of cast iron. Metals **15**, 214 (2025). https://doi.org/10.3390/met15020214
74. V. Claremboux, S.K. Kawatra, Iron ore pelletization: Part III. organic binders. Miner. Process. Extr. Metall. Rev. **44**, 138–154 (2023). https://doi.org/10.1080/08827508.2022.2029431
75. R.D. Morales, L.G. Rubén, F. López et al., The slag foaming practice in EAF and its influence on the steelmaking shop productivity. ISIJ Int. **35**, 1054–1062 (1995). https://doi.org/10.2355/isijinternational.35.1054
76. P. Paknahad, M. Askari, S.A. Shahahmadi, Cold-briquetted iron and carbon (CBIC), investigation of steelmaking behavior. J. Mater. Res. Technol. **9**, 6655–6664 (2020). https://doi.org/10.1016/j.jmrt.2020.04.058